# Electron cloud generation and trapping in a quadrupole magnet at the Los Alamos proton storage ring

Robert J. Macek,* Andrew A. Browman, and John E. Ledford

*TechSource, Inc., Santa Fe, New Mexico 87505, USA*
*and Los Alamos National Laboratory, Los Alamos, New Mexico 87545, USA*

Michael J. Borden, James F. O'Hara, Rodney C. McCrady, Lawrence J. Rybarcyk,
Thomas Spickermann, and Thomas J. Zaugg

*Los Alamos National Laboratory, Los Alamos, New Mexico 87545, USA*

Mauro T. F. Pivi

*Stanford Linear Accelerator Center, Menlo Park, California 94025, USA*

Recent beam physics studies on the two-stream e-p instability at the LANL proton storage ring (PSR) have focused on the role of the electron cloud generated in quadrupole magnets where primary electrons, which seed beam-induced multipacting, are expected to be largest due to grazing angle losses from the beam halo. A new diagnostic to measure electron cloud formation and trapping in a quadrupole magnet has been developed, installed, and successfully tested at PSR. Beam studies using this diagnostic show that the "prompt" electron flux striking the wall in a quadrupole is comparable to the prompt signal in the adjacent drift space. In addition, the "swept" electron signal, obtained using the sweeping feature of the diagnostic after the beam was extracted from the ring, was larger than expected and decayed slowly with an exponential time constant of 50 to 100 $\mu$s. Other measurements include the cumulative energy spectra of prompt electrons and the variation of both prompt and swept electron signals with beam intensity. Experimental results were also obtained which suggest that a good fraction of the electrons observed in the adjacent drift space for the typical beam conditions in the 2006 run cycle were seeded by electrons ejected from the quadrupole.

## I. INTRODUCTION

Electron cloud effects (ECE), including an electron cloud-induced instability, have long been observed at the Los Alamos Proton Storage Ring (PSR) [1–3]. While this high-current (120 $\mu$A average current), medium energy (800 MeV) accumulator ring is used mainly to drive a short-pulse spallation neutron source (at 20 Hz repetition rate) for the Lujan Neutron Scattering Center at Los Alamos [4], PSR has also proven to be a useful test bed for the study of ECE in long-bunch proton rings. For a list of other accelerator parameters, see Table I.

A fast, transverse, beam instability has been observed at PSR from the time it was first commissioned in 1985. Considerable evidence has been accumulated showing that it is a two-stream instability driven by coupled motion of the proton beam with low-energy clouds of electrons, hence the designation "e-p" instability [5,6]. A major remaining issue is development of a more complete and self-consistent picture of the dominant sources of the electron clouds driving the instability. Such an understanding would be beneficial for the development of a cure by suppression of the dominant sources of electron clouds.

Past studies at PSR, using the Harkay-Rosenberg retarding field analyzer (RFA) detectors [7] and a LANL variant that adds a sweeping electrode [8], have produced compelling evidence for the generation of significant electron clouds by beam-induced, "trailing edge multipactor" of "seed" electrons born at the wall in drift spaces [6,9]. For example, simulations made assuming a constant production rate (per lost proton) for primary or seed electrons from beam losses uniformly distributed around the ring reproduced a number of important features of the RFA measurements in drift spaces at PSR [9], including the time profile (pulse shape) and energy spectrum of electrons striking the wall (prompt electron signal) as well as the approximate signal amplitude. In addition, biased collection electrodes in a PSR quadrupole and dipole showed evidence for electron cloud generation in these components but the data are more difficult to interpret because the biased electrodes distort the beam-induced multipactor process.

Several methods to mitigate the instability by suppression of the electron cloud in selected drift spaces at PSR were tried and have not lead to a cure, which suggests that the dominant sources are in other components. Electron clearing by biasing the stripper foil to ~10 kV and use of clearing electrodes (biased up to ±20 kV) of various lengths in 8 of the 10 drift spaces between quadrupole

---
*macek@lanl.gov

TABLE I.   PSR parameters.

| Parameter | Symbol | Value |
| --- | --- | --- |
| Beam kinetic energy | $T$ | 798 MeV |
| Betatron tunes | $\nu_x, \nu_y$ | 3.19, 2.19 |
| Incoherent tune shifts at 100 $\mu$A | $\Delta\nu_x, \Delta\nu_y$ | $-0.22$, $-0.18$ calculated |
| Chromaticities | $\xi_x$ | $-1.22 \pm .07$ measured, $-0.8$ calculated |
| (normalized) | $\xi_y$ | $-1.14 \pm .06$ measured, $-1.3$ calculated |
| Transition gamma | $\gamma_T$ | 3.1 |
| Phase slip factor | $\eta$ | $-0.19$ |
| Maximum rf voltage | $V_{\mathrm{rf}}$ | 18 kV |
| Synchrotron tune (at 10 kV) | $\nu_0$ | 0.000 42 |
| Buncher harmonic, frequency | $h, f$ | 1, 2.795 MHz |
| Beam bunch length | | Up to 300 ns or 75.7 m |
| Mean pipe radius | $b$ | 0.05 m |
| Circumference | $C = 2\pi R$ | 90.26 m |

magnets had a marginal effect ($\sim 10\%$–$15\%$ change) on the instability threshold for bunched beams but may be consistent with the total length of the clearing electrodes ($\sim 16\%$ of the ring circumference) [10–12]. The use of weak solenoidal magnetic fields suppressed (by a factor of $\sim 50$) the prompt electron signals from an RFA embedded in a short test section of PSR. However, when solenoid windings were installed over $\sim 10\%$ of the circumference, i.e., 3 of the 10 drift spaces between quadrupoles at PSR, they had no effect on the instability threshold [13].

The largest uncertainty in the prediction or simulation of electron cloud generation in the various components of a long-bunch proton machine, such as PSR, is reliable knowledge of the number and distribution of primary electrons that are then amplified by a beam-induced multipactor. Beam loss monitors and activation measurements provide some general information on the location and amount of beam loss, but accurate information on the angle of incidence of the lost protons with the chamber walls is nearly impossible to obtain. Such information is crucial since the number of electrons produced per lost proton is a strong function of the angle that the lost proton makes with the chamber wall [14] i.e. the number varies $\sim 1/\cos(\theta)$ (where $\theta$ is the angle of incidence with respect to the normal to the surface).

Other sources of seed electrons are possible including electrons produced at the stripping foil and those related to residual gas ionization. Primary electrons from residual gas ionization by the beam are born near the beam in the center of the pipe and therefore have the lowest multipactor gain and, in addition, not many are produced at typical PSR operating vacuum conditions ($\sim 10^{-8}$ Torr). Ions produced by beam interactions with the residual gas will be repelled by the beam and strike the wall with up to 2 keV of kinetic energy and can also produce small numbers of seed electrons at the wall.

As a result of the above-mentioned considerations, we have concluded that it will be necessary to measure elec-tron cloud generation in components other than drift spaces if we are to reliably identify the dominant sources of electron clouds that drive the e-p instability in PSR. We have for some time suspected that quadrupoles may be a strong source of electron clouds in PSR. From analytical models [15] and the simulations, we know that the primary electrons born at the wall in PSR have the highest multipactor amplification. Since the number of electrons produced per lost proton varies as $1/\cos(\theta)$, we look for regions of grazing angle beam losses. Beam tracking studies with the ORBIT code [16,17] show that grazing angle losses (from Coulomb scattering in stripper foil) will be largest in the quadrupoles where the beam sizes are at a local maximum and much lower elsewhere. Other reasons to suspect quadrupoles include the data from biased collection electrodes taken in 1999 which showed a larger signal from a quadrupole than in a dipole or drift. Furthermore, the strip detector in an SPS quadrupole at CERN gave a larger signal than measured for a dipole or a drift [18]. Significant electron clouds have also been observed in quadrupole transport for other accelerators, e.g., the high-current experiment using a 1 MeV $K^+$ beam at LBNL [19]. Other studies of ECE in quadrupoles include a study at KEKB of the effect of weak solenoids (in quadrupole magnets) on the electron cloud instability [20]. No clear effect was observed, however, the result is consistent with simulations which showed that the 17 G solenoid field used in the experiment has no effect on the central electron cloud density. A direct measure of the electrons by a suitable diagnostic in quadrupoles is needed to resolve the issue.

Simulations of the electron cloud development in a PSR quadrupole were made using a modified version of the POSINST code [9,15] and showed several important effects that guided our planning: (i) The amplification of primary electrons in quadrupoles was about a factor of $\sim 25$ less than in drift spaces for the same beam; however, this effect may be more than compensated by the high primary elec-

tron production rate from grazing angle losses in the quadrupole. (ii) Electrons can be trapped in the magnetic fields of the quadrupole with long decay times. These could enhance the density of electrons surviving the passage of the beam-free gap between bunch passages and thus contribute to electrons that drive the e-p instability. (iii) Numerous electrons were ejected from the quadrupole by the $E \times B$ drift mechanism into the adjacent drift spaces.

The latter effect was subsequently verified by an analytical calculation. This suggests that electrons ejected from the quadrupole magnet, rather than those produced directly from beam losses in the drift space, may be the main source of seed electrons for the adjacent drift spaces. These will subsequently be amplified by a trailing edge multipactor in the drift space.

## II. QUADRUPOLE DIAGNOSTIC

To study electron cloud generation and trapping in a PSR quadrupole, we have developed a diagnostic which can measure the electron flux striking the wall during a beam-induced multipactor (the prompt electron signal), and by pulsing a sweeping electrode can also measure electrons trapped in the quadrupole after the beam pulse has left the magnet [21]. A schematic cross-sectional diagram of the diagnostic is shown in Fig. 1. Photographs of the device and selected components as fabricated are shown in Figs. 2–4.



FIG. 2. (Color) Detector assembly before installation in the quadrupole magnet. Labeled components include the RFA chamber with vacuum cover plate, the sweeping electrode housing (cover), and the signal connector to the collector plate.



FIG. 3. (Color) Interior surfaces of diagnostic showing the stainless steel RFA entrance plate and the HV sweeping electrode.

The diagnostic is an adaptation of the electron sweeping detector which we developed earlier for use in drift spaces [8]. Electrons from the cloud execute gyromotion (typical radius <1 mm) around magnetic (B) field lines in the
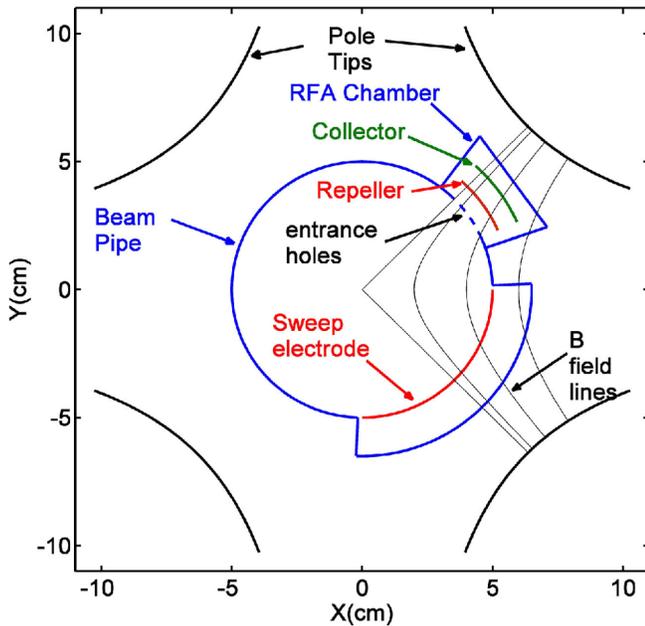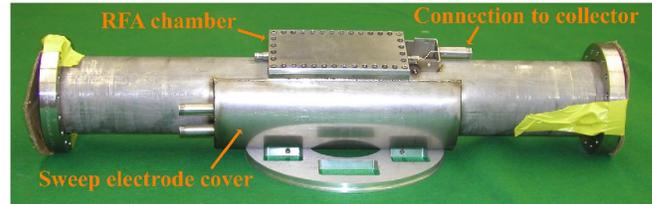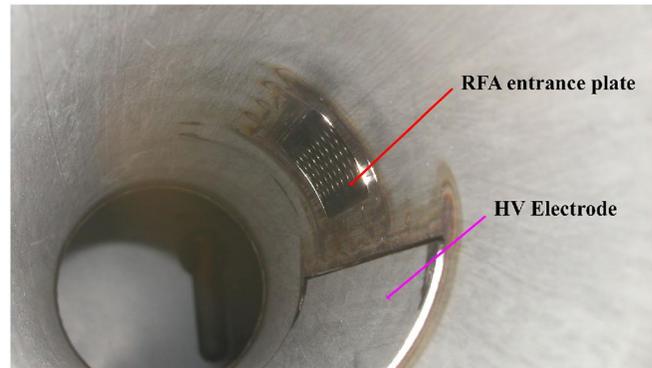


FIG. 1. (Color) Schematic cross section of the electron sweeping diagnostic in a quadrupole magnet. Its principal components are an RFA chamber containing a repeller grid and collector plate concentric with the circular beam pipe, holes in the beam pipe at the entrance to the RFA chamber, and a high voltage sweeping electrode.
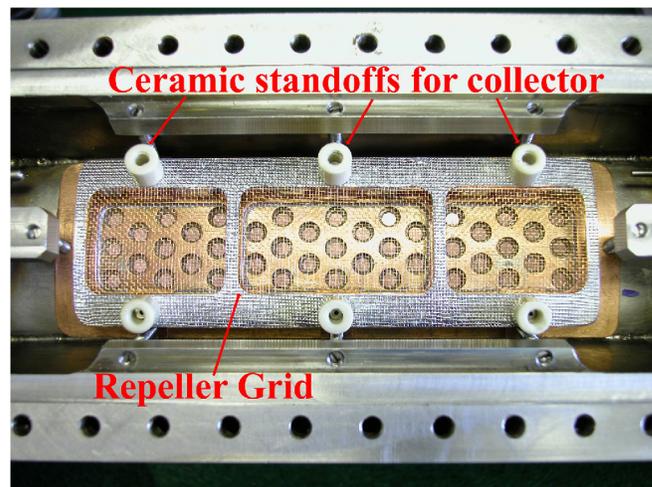


FIG. 4. (Color) View of the RFA chamber with flange cover removed. Visible components include the stainless steel RFA entrance plate (2.8 mm holes) which is covered with a copper plate with slightly larger holes, the repeller screen mounted on rf capacitors beneath the screen, and ceramic standoffs to which the collector plate will be attached.

ROBERT J. MACEK *et al.*

Phys. Rev. ST Accel. Beams **11,** 010101 (2008)

quadrupole field and can enter the RFA chamber through holes in the beam pipe. They will get past the repeller grid if they have sufficient velocity along the magnetic field lines to overcome the negative bias (Vrep) on the repeller grid and will be collected at the collector plate to produce the detector signal. The collector plate is biased to +45 V to suppress secondary electron emission at the collector. Wide bandwidth (1 kHz to 50 MHz) front end electronics are placed close to the magnet in the beam tunnel, as shown in Fig. 5, to amplify the collector signal for observation and recording outside of the beam tunnel.

Electrons trapped or remaining in the quadrupole field can be observed by pulsing the sweeping electrode with a fast rise time negative voltage pulse (typically −485 V) when the beam is not present in the magnet (during the beam-free gap passage or after extraction). The signal produced by pulsing the sweeping electrode is designated the ''swept electron'' signal to distinguish it from the ''prompt signal'' (generated during the multipactor process) obtained when the sweeping electrode is grounded.

Previous experience with fast amplifiers on the collector signal showed it was necessary to give careful attention to reducing electromagnetic pickup from the beam. The en-

trance holes to the RFA chamber were 2.8 mm in diameter with spacing between them sufficient to have the holes represent ∼20% of the surface area at the entrance. This configuration accomplishes two objectives; (1) it leaves most of the metal intact to carry wall currents with little additional impedance and (2) is a reasonable trade off between signal strength (electron flux reaching the collector) and reduction of the multipactor gain in this region from the reduced effective secondary emission yield (SEY) resulting from the area of the holes which do not emit secondary electrons. In addition, the entrance plate was covered with 40 mesh copper screen sandwiched between the entrance plate and a copper plate with somewhat larger holes aligned with the holes in the entrance plate. The screen was soldered to both the stainless steel entrance plate and the copper covering plate. The copper cover plate was pressed firmly to the surrounding beam tube by 8 set screws which can be seen in Fig. 4. The repeller grid screen was soldered to 12 ceramic chip rf capacitors which gave a good rf (AC) ground to the repeller grid at the higher frequencies of interest. Larger capacitors were added in a capacitor box (see Fig. 5) ahead of the front end electronics module to bypass lower frequencies at the repeller. Even with these measures, significant beam pickup was observed. Fortunately, the beam pickup was sufficiently reproducible from pulse to pulse to allow a background subtraction to greatly improve the signal to noise ratio.

## III. EXPERIMENTAL RESULTS

The electron cloud diagnostic works well and provides good quality signals using background subtractions (obtained with repeller at −511 V) and averaging over 16 to 64 macropulses (i.e., accumulation cycles in the ring). Using this device, we were able to obtain good measurements of the prompt and swept (trapped) electron signals and thereby better characterize the generation and trapping of electron clouds in a quadrupole magnet. Measurements were made of the effect on the electron cloud signal of changing several beam and accelerator parameters including variation of beam intensity, beam emittance, momentum spread, rf buncher voltage, changes in local beam losses, closed orbit offsets in the region of the quadrupole, changes in vacuum pressure, and proximity to the e-p instability threshold. In the following sections we will present the most significant results.

### A. Electron signals from the diagnostic

An example of prompt and swept signals for a production beam of 86 $\mu$A (4.29 $\mu$C/pulse at 20 Hz) is shown in Fig. 6 and compared to the proton beam current measured by a wall current monitor (designated WC41). Electrons from a trailing edge multipactor give a prompt signal that peaks at the end of each proton beam pulse passage. The swept signal was produced by applying a short ( ∼ 100 ns) −485 V pulse to the sweeping electrode ∼3.5 $\mu$s after the



FIG. 5. (Color) Diagnostic installed in quadrupole magnet (SRQU41) in the ring tunnel. The front end electronics module is attached to the side of the quadrupole magnet. The end field region of the adjacent dipole is also visible.
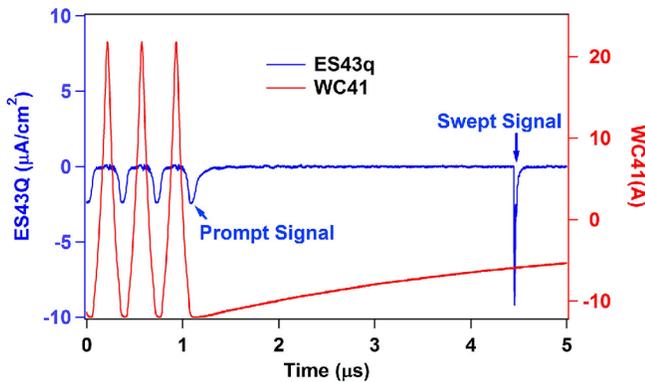
FIG. 6. (Color) Prompt and swept electron signals from quadrupole detector (designated as ES43Q) for a 4.29 $\mu$C/pulse beam (10/31/06) compared with the proton beam current measured with the wall current monitor (WC41). For this graph the electron detector signal has been converted to an electron flux ($\mu$A/cm$^2$) striking the wall at the entrance to the RFA chamber.
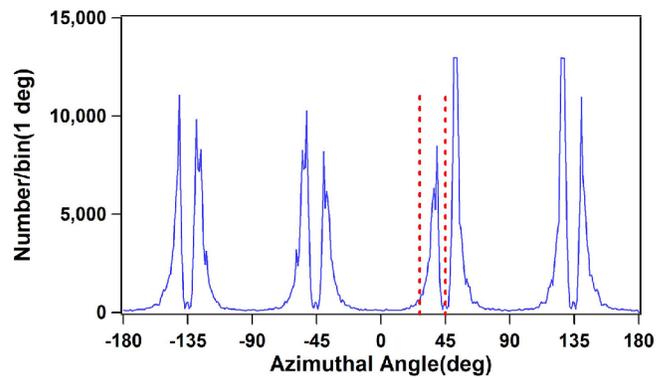


FIG. 7. (Color) Histogram of simulation results for the azimuthal angular distribution of electrons striking the wall in a quadrupole magnet. The vertical red lines show the 18 degree angular region (27 to 45 degrees) for the entrance holes of the quadrupole diagnostic.

beam was extracted. In typical operation of both the quadrupole diagnostic (ES43Q) and the drift diagnostic (ES41Y), the repeller voltage is set to $-11$ V except when data is being collected for a prompt electron energy spectrum. This voltage is chosen rather than 0 V mainly to avoid problems with regulation of the bias supply when the magnitude of the bias is below 10 V. To obtain data with 0 V bias on the repeller, the bias supply is replaced with a termination that connects the repeller screen to ground potential.

When the prompt signal is converted to an electron flux striking the wall (using the area of the entrance holes, the transmission of the ground and repeller screens, and the transimpedance of the amplifiers), we find the important result that the electron flux striking the walls in the quadrupole is $\sim$1 to 3 times larger than the flux measured in an adjacent drift space. Since simulations indicate that the beam-induced multipactor gain for electrons is about a factor of 25 or so lower in a quadrupole than in a drift space, we now have evidence that the flux of seed electrons generated by beam losses in the region of the electron detectors is considerably higher (factor of 25 or more) in the quadrupole than in the adjacent drift space for typical beam conditions present in the 2006 run cycle. The evidence would be more definitive with better information on the angular distribution of the electron flux striking the walls at the two detector locations so that the fluxes integrated over the transverse circumference of the pipe could be determined.

Some information on the angular distributions is available. Measurements of the electron flux in the vicinity of the drift space detector were made in 2001 with two identical RFA devices, one in the vertical plane and the other in the horizontal plane. In these measurements, the vertical signal was a factor of $\sim$10 larger than the horizontal which indicates that most of the electron flux strik-

ing the wall in the drift space detector is concentrated in the vertical direction. The simplest estimate of the average flux would be the average of the horizontal and vertical measurements or about a factor of 0.55 times the vertical flux. For the quadrupole region, simulations of the electron flux striking the wall for a beam intensity of 8 $\mu$C/pulse and a uniform angular distribution of seed electrons show a split peak at each of the pole tips as shown in Fig. 7. The asymmetry in the split peaks, particularly near 45 and 135 degrees, may be due to the asymmetry of the beam potential arising from the elliptical beam spot which has dimensions 4.5 mm (rms) in the horizontal plane and 12 mm (rms) in the vertical. The 18 degree coverage of the diagnostic intercepts $\sim$9% of the simulated flux integrated over the circumference of the pipe and covers 5% of the circumference, thus the average flux is $\sim$0.45 times the flux measured at the quadrupole diagnostic in its present orientation. With these assumptions for the angular distributions at the two detectors, the average flux at either detector is about half the flux determined from their respective prompt signals. Using these average fluxes, the conclusion in the previous paragraph remains the same.

### B. Electrons trapped in the quadrupole

A key motivation for the development of this diagnostic was to measure the line density and lifetime of electrons trapped in the quadrupole after the beam is extracted. Plots of the trapped (swept) electron signal amplitude as a function of time after extraction from the quadrupole detector are presented in Fig. 8 and show that the trapped electrons persist for a long time (200–300 $\mu$s) with an exponential decay time of $\sim$60 to 90 $\mu$s.

The measured decay time ($\sim$ 100 $\mu$s for the 7.1 $\mu$C beam pulse) is in reasonable agreement with simulations but the measured ratio of the swept signal amplitude (at $\sim$5 $\mu$s after extraction) to the last prompt signal is considerably larger (factor of 5–10) than obtained in simula-
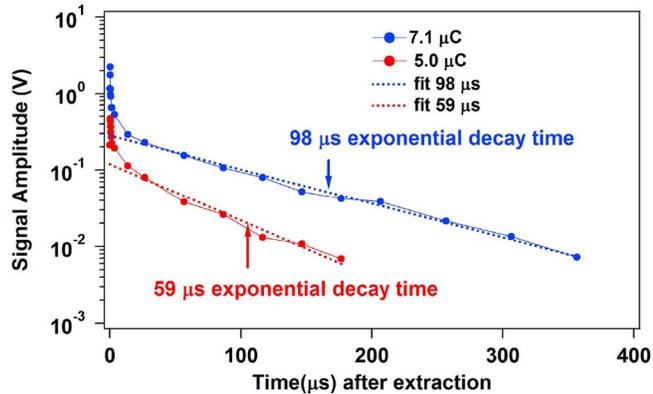
FIG. 8. (Color) Trapped electron dissipation/decay curves for ES43Q amplitude data of 9/16/06 taken at two beam intensities, 7.1 $\mu$C/pulse and 5.0 $\mu$C/pulse. The exponential decay times shown were obtained from fits to the portion of the curves after $\sim$15 $\mu$s.

tions. The integral of the swept electron signal obtained near the end of the $\sim$80 ns beam-free gap between bunch passages translates into a line density of $\sim$0.6 nC/m compared with an average proton line density of $\sim$95 nC/m for the 7.1 $\mu$C beam pulse.

### C. Signal variation with beam intensity

Both swept and prompt electrons signals were measured as a function of beam intensity while holding all other beam control parameters fixed. Beam intensity was varied by ''chopping'' (removing) one out of $n$ turns of injection into the ring. All other parameters such as the linac settings, injection offset, accumulation time, rf buncher voltage, etc. were kept fixed. Plots of the data for the prompt and swept signal amplitudes as a function of beam intensity are shown in Fig. 9 along with power law fits to the data. Both signal amplitudes vary strongly with intensity; the data fitting gave exponents of 5.2 and 3.6 for the prompt
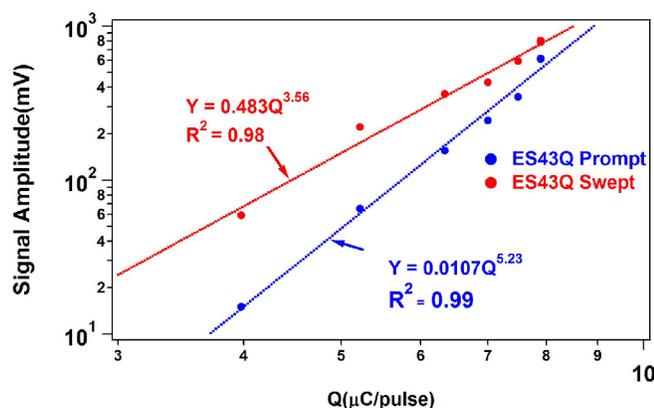


FIG. 9. (Color) Variation with beam intensity of prompt and swept signals from the quadrupole diagnostic (ES43Q) (9/16/06).

and swept signal curves, respectively. Simulations of the prompt signals at two intensities (5 and 8 $\mu$C/pulse) for a peak SEY of 1.5 and constant fractional beam loss rate (lost protons/circulating protons) show much less variation with intensity. In this case, the simulations gave a value of 2.46 for the ratio of the prompt signal amplitude at 8 $\mu$C/pulse to that at 5 $\mu$C/pulse, which is to be compared with a ratio of 11.7 from the data of Fig. 9.

A similar behavior was observed for measurements in a drift space in 2001. The power law exponents were even higher and the only way to get agreement with simulations was to assume that the seed electron generation was exponential with intensity rather than proportional to intensity. The latter simulation work was studied by Yoichi Sato in his Ph.D. thesis and reported in his talk at the ECLOUD'07 workshop [22].

### D. Signal variation with beam loss

By moving the injection stripper foil about 1 mm in both the horizontal and the vertical direction, we increased the number of stored beam foil hits by a factor of about 3 as measured by the increase in foil current. This increases the beam losses from foil scattering (nuclear and large angle Coulomb scattering) by the same factor without affecting any other beam parameters including the ''first turn'' beam losses from the production of excited states of $H^0$ (principal quantum number, $n \geq 3$) which field strip part way into the first dipole downstream of the stripper foil and are lost from the ring acceptance. The beam halo and emittance growth from space charge effects would also be unaffected. With these beam loss variations, we observed that the prompt signal amplitude from ES43Q increased by approximately the same factor (2.3), thus demonstrating that foil scattering losses are a major factor in the production of seed electrons in the quadrupole.

### E. Prompt electron energy spectra

Information on the energy spectra of prompt electrons in the quadrupole diagnostic was obtained from signal amplitudes measured using different bias voltages (Vrep) on the repeller grid. In the approximation that the magnetic field of the quadrupole is uniform between the beam pipe and repeller grid over the small angular region covered by the entrance holes, then electrons having an energy component along the B field (designated as the longitudinal energy) less than the repeller bias potential will not get past the repeller grid. Therefore, the resulting prompt signal consists of electrons with longitudinal energy greater than the repeller bias thereby providing a measurement of the cumulative longitudinal energy distribution. Results of energy spectra measurements (taken 11/18/06) are plotted in Figs. 10 and 11 for two beam intensities, 5 and 7 $\mu$C/pulse, and compared with simulations, which also computed the longitudinal energy component along the magnetic field at the entrance to the RFA chamber.

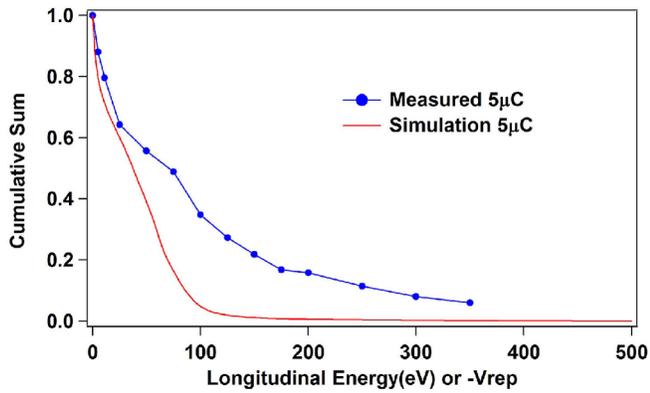FIG. 10. (Color) Prompt electron cumulative longitudinal energy spectrum from the quadrupole diagnostic for a beam intensity of 5 $\mu$C/pulse. The abscissa for the measured distribution is $-$Vrep (repeller voltage) and the curve is normalized to 1 at Vrep $= 0$.
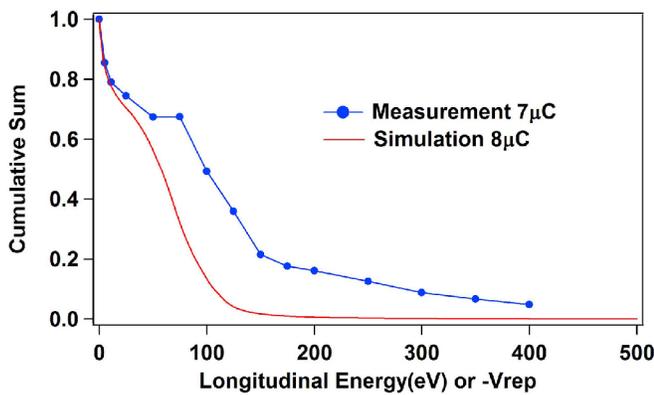


FIG. 11. (Color) Prompt electron longitudinal cumulative energy spectrum from the quadrupole diagnostic for a beam intensity of 7 $\mu$C/pulse compared with simulation results for a beam intensity of 8 $\mu$C/pulse. The abscissa for the measured distribution is $-$Vrep (repeller voltage) and the curve is normalized to 1 at Vrep $= 0$.

In both Figs. 10 and 11, the measured distributions show a median electron energy (energy where the cumulative distribution $= 0.5$) that is 50% or so higher than for the distributions from simulations. The reason for this discrepancy is not yet understood but may be related to using a seed electron distribution that was uniform in its azimuthal distribution in the quadrupole rather than a more realistic distribution strongly peaked in the vertical direction. Future modifications to the simulation code will incorporate an arbitrary distribution of seed electrons.

### F. Evidence for electrons ejected from quadrupole

Another electron cloud diagnostic (labeled ES41Y RFA) located in the drift space just upstream of the quadrupole was used in conjunction with the quadrupole diagnostic
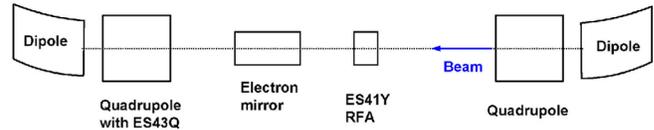


FIG. 12. (Color) Schematic layout (not to scale) of the section where electron cloud measurements (discussed in this paper) were made. The drift space between quadrupoles is 4.2 m and effective length of each quadrupole is 0.5 m.

(ES43Q) to obtain evidence for electrons ejected from the quadrupole. A schematic layout of ring components in this region is shown in Fig. 12.

A significant reduction ($\sim 25\%$) of the prompt electron signal (ES41Y) in the nearby drift space was observed when the sweeping electrode in the quadrupole was pulsed at $-485$ V for 2–3 $\mu$s while beam was still present in the ring as shown in Fig. 13. Such a reduction would be expected if a significant fraction of the drift space signal is seeded by electrons ejected from the quadrupole rather than directly by beam losses in the drift space near the electron diagnostic. Pulsing of the sweeping electrode in the quadrupole will suppress some electron generation during multipacting and will also clear out electrons trapped in the quadrupole in the region near the electrode during passage of the gap between bunch passages. This will then reduce the electrons ejected from the quadrupole by the E $\times$ B drift mechanism while the electrode has $-485$ V impressed on it.

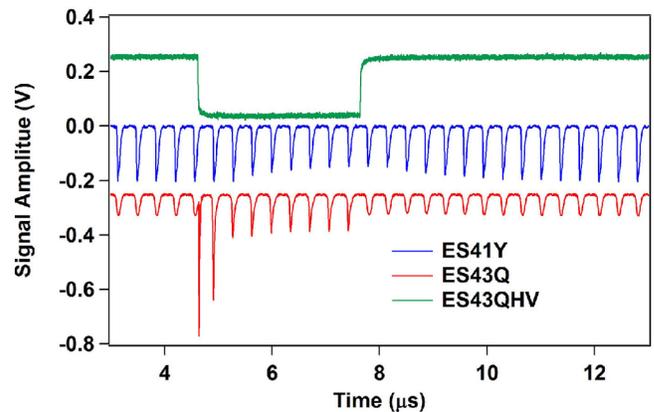The decay and recovery of the ES41Y signal in response to sweeping the electrode in the ES43Q detector takes



FIG. 13. (Color) Evidence for seeding of the drift space region by electrons ejected from the quadrupole (10/16/07). The green curve (ES43QHV) is an attenuated signal from the $-485$ V pulse applied to the sweeping electrode in the quadrupole. The corresponding collector signal from the quadrupole is the red curve (ES43Q). The blue trace is the prompt signal from the ES41Y detector in the adjacent drift space. Note the $\sim$25% reduction in the ES41Y signal after about 8 turns with the sweeping electrode energized followed by recovery after the electrode is deenergized.

several turns ( ∼ 1.5 $\mu$s) as can be seen in Fig. 13. The recovery time for this situation is comparable to the time it takes the prompt signal at ES41Y to recover from sweeping the gap with one short, 100 ns pulse using the ES41Y sweep electrode [13]. It is also of interest to compare these times with the much faster time ( ∼ 100 ns estimate from simulations) for electrons ejected from the quadrupole to reach the ED41Y detector. A satisfactory explanation for the several turn recovery phenomenon has not yet been established but is likely related to the time it takes to reestablish equilibrium after a rapid change to the electron cloud density in a particular region. Cold electrons captured by the beam at the end of the gap (between bunch passages) do not participate in a trailing edge multipactor but are released at the end of the beam pulse where they can have sufficient energy to create an additional set of secondary electrons. Buildup from this mechanism can take several turns to reach equilibrium. This issue has been examined by Sato in his Ph.D. thesis [23].

While the results shown in Fig. 13 are typical for well-tuned production beams in the 2006 run cycle, there were significant day-to-day variations (up to a factor of 2 reduction in the effect) which have not yet been studied systematically. Simulations of this experiment will be undertaken in the future.

### G. Results with an electron mirror

To further test the hypothesis that electrons ejected from the quadrupoles are a major source of seed electrons in the drift space, we constructed and installed a longitudinal barrier to electrons moving along the beam axis between the quadrupole and the drift space electron detector. We named the barrier an electron "mirror" or "electron suppressor ring." A longitudinal cross section diagram for the mirror is shown in Fig. 14. The mirror assembly consists of a short (30 cm) metal tube insulated from the beam chamber using Macor® rings. The metal tube can be biased or pulsed with negative voltage to prevent electrons ejected from the quadrupole from reaching the drift space detector.

A plot of the electrostatic potential (calculated with the SUPERFISH code) as a function of longitudinal position from the device center is shown in Fig. 15. The center
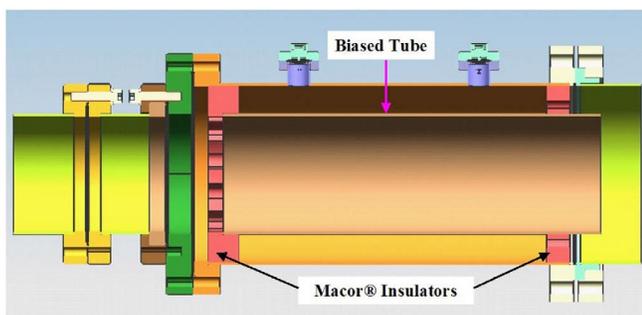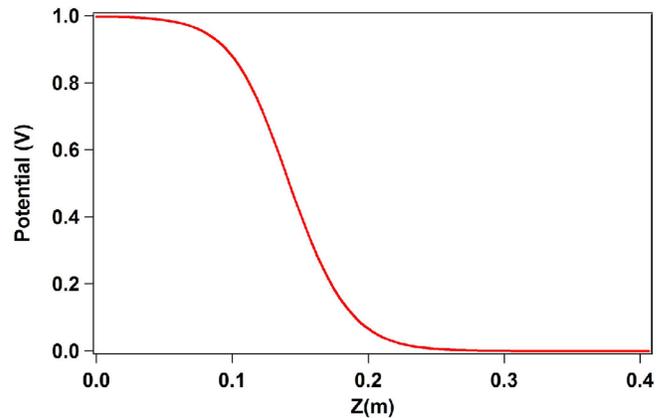


FIG. 15. (Color) Plot of the on-axis electrostatic potential for the mirror as a function of longitudinal position starting from the center of the mirror tube. A voltage of +1 V was applied to the mirror tube.

tube of the mirror is set at a voltage of +1 V for this numerical calculation.

We planned two such devices to be installed, one on each side of the drift space electron detector, in order to suppress electrons ejected from both the upstream or downstream quadrupoles. With these barriers biased appropriately, the remaining signal from the drift space detector would be that due to seed electrons generated by direct beam losses in the region of the drift space electron detector. However, we only had time and resources to construct, install, and test one such device with beam before the PSR operation was shut off for an extended maintenance outage on December 22, 2006. The one mirror was installed between the quadrupole and the drift space diagnostic (ES41Y) as shown in the Fig. 12 layout.

The effect on the ES43Q and ES41Y prompt signals when biasing the one mirror is shown in the voltage scan of Fig. 16 for a beam intensity of 4 $\mu$C/pulse (taken 11/23/06). The peak in the ES41Y signal around a mirror
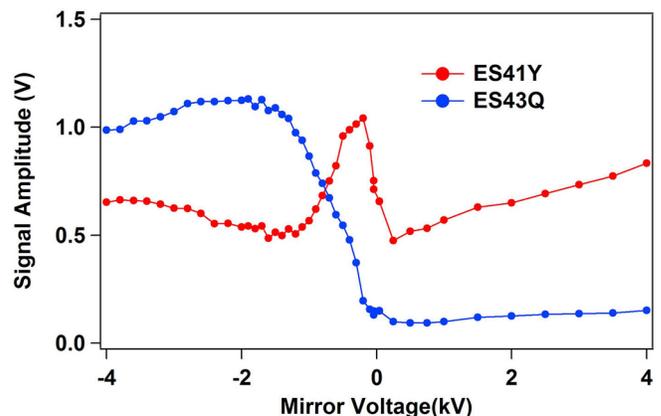


FIG. 16. (Color) Mirror voltage scan showing the prompt signal amplitudes from the quadrupole diagnostic (ES43Q) and the drift space diagnostic (ES41Y) as a function of voltage (kV) applied to the electron mirror.



FIG. 14. (Color) Section of electron mirror along the beam axis.

voltage of $-300$ V was not anticipated; however, we note that this signal is a delicate balance between suppressing electrons ejected from the downstream quadrupole and reflecting electrons ejected from the upstream quadrupole back to drift space diagnostic and is therefore sensitive to the imbalances.

The peak in the ES41Y signal largely disappeared when a similar scan was made at 7 $\mu$C/pulse. Predicting this curve by simulation undoubtedly requires the capability for dealing with more than one magnet and using lattice functions that vary with position, both of which are features not yet incorporated in the code.

For the prompt ES43Q signal from the quadrupole diagnostic, the unexpected and surprising result was a *large increase (typically a factor of 5 to 10)* in the electron signal when the mirror was biased with negative voltage between $-1000$ and $-4000$ V. A comparable increase was seen in the swept (trapped) electron signal in mirror scans for an 8 $\mu$C/pulse beam taken on another occasion where both prompt and swept signals were recorded for the same beam pulses. One possible explanation for the increased signal is that electrons reflected from the mirror enter the quadrupole via the $E \times B$ drift mechanism in time to undergo a trailing edge multipactor in the quadrupole. Our modified version of POSINST 12.1 does incorporate the static mirror field in a model using one quadrupole, but simulations with this version showed no significant increase in the prompt signal at the quadrupole. This discrepancy suggests that some important physics is missing in the model.

## IV. SIMULATIONS OF THE MEASUREMENTS

Simulations of the various measurements made with the quadrupole diagnostic are under way using a modified version of the POSINST 12.1 code [9]. At the present time, the model uses a uniform longitudinal distribution of primary electrons along the quadrupole magnet and for the angular distribution around the beam pipe uses either a uniform distribution or one weighted according to the transverse beam dimensions. Version 12.1 included a 3D model for the quadrupole field [15] to which we have added a 2D electrostatic model for the sweeping electrode

electric field, a 2D axially symmetric electrostatic model for the electron mirror field (see Fig. 14 for a plot of the normalized potential), and segmented slots ("black holes") for the entrance holes to the RFA chamber. Other features and the key parameters used in the simulations discussed in this paper are listed in Table II below.

Our comparisons with data are just beginning, thus only a subset of the data has been simulated. The time profile of the prompt and swept signals is in reasonable agreement with measurements but, as noted earlier, the amplitude ratio of swept and prompt signals disagrees with measurement by a factor of 5 to 10. The dissipation of electrons trapped in the quadrupole after beam is extracted is in reasonable agreement with simulations for the $\sim 7$ $\mu$C/pulse beam, i.e., the behavior is exponential $\sim 10$ $\mu$s after extraction and beyond with a decay constant of $\sim 100$ $\mu$s.

Simulations of the prompt electron cumulative energy spectra for the quadrupole diagnostic were compared with data in Figs. 10 and 11. In both cases the median electron energy from the measurements was significantly higher (50% or more) than the median energy from the corresponding simulation. The reason for this discrepancy is not yet determined. It may be due to subtle changes in the longitudinal shape of the beam pulse especially on the trailing edge or possibly from the uniform angular distribution of seed electrons used in the simulation. Future work will use the measured longitudinal beam profile taken at the same time as energy spectra along with a more realistic angular distribution of seed electrons obtained from ORBIT simulations of the PSR which included scattering in the stripper foil.

Simulations using just one quadrupole and the electron mirror with seed electrons generated only in the quadrupole did not produce the large increase in the prompt signal seen in the data of Fig. 16. It may be the result of not using the proper distribution of seed electrons; or the nearby dipole end fields may also play a role. We know that the longitudinal and transverse distribution of seed electrons used in the present simulations do not agree with beam loss distributions from beam tracking codes. Beam particle tracking in ORBIT shows that grazing angle losses in the

TABLE II.   Parameters used in the simulations.

| Parameter | Value |
|---|---|
| $\delta_{max}$ (maximum value of SEY) | 1.5 |
| Beam intensity | 5 or 8 $\mu$C/pulse |
| Longitudinal beam distribution | Average shape measured 10/7/2001 |
| Fractional proton loss rate | $4.44 \times 10^{-8}$/m/circulating proton |
| Seed electrons per lost proton | 100 |
| Angular distribution of seed electrons | Uniform or weighted by beam spot dimensions |
| Transverse beam distribution | 2D Gaussian |
| Beam spot dimensions (rms) | 4.5 mm horizontal, 12 mm vertical |
| Vacuum pressure | $10^{-8}$ Torr |

quadrupole containing the EC diagnostic are very strongly peaked in the vertical direction (azimuthal angles near $\pm 90°$), whereas the POSINST 12.1 model uses either a uniform distribution or one weighted by the beam transverse dimensions.

Another serious limitation of simulation model, at least for a small ring such as PSR, is that it only handles one accelerator element at a time and with no variation of lattice functions with longitudinal position. Because electrons ejected from the quadrupole have significant longitudinal motion (several meters of travel) during one bunch passage, the model needs to handle more than one element. In particular, the end fields of the dipole next to the quadrupole slightly overlap the fringe field of the quadrupole. Since the end fields of the dipole have gradients, they can also impart $E \times B$ drifts to electrons and send some back into the quadrupole. In addition, the two quadrupoles are separated by only 4 m of drift and some of the electrons ejected from one quadrupole can reach the other quadrupole and be injected into it. It is clear that with significant longitudinal motion of electrons from quadrupoles and dipole end fields, interactions between ring elements should be included in the simulations and their importance investigated.

Our experience-based insight to date suggests that we need to add a number of other features to the model such as a more general pattern of seed electrons that can be a tabulated function of longitudinal position and azimuth transverse to the beam chamber (e.g. obtained from ORBIT simulations of beam losses in the ring). A capability to model a section of the ring with multiple elements and the corresponding variations of lattice parameters is desirable. In particular, we see the need to include two quadrupoles and the end fields of the dipole which slightly overlap the fringe field of the adjacent quadrupole. We plan to eventually model a section which consists of two dipole end fields with nearby quadrupoles and the drift space between the two quadrupoles where the electron mirrors and drift space electron diagnostic are located.

One of the greatest uncertainties in simulation or modeling of the electron cloud formation in the PSR is the number and distribution of primary electrons. Unlike the short-bunch, long train storage rings such as the CERN SPS or positron rings of the B-factories, the buildup of the prompt signal on the trailing edge of the PSR bunch does not appear to saturate at presently available bunch intensities. In the former, the buildup saturates part way through the bunch train and the final value is determined by space charge neutralization of the beam and not on the number of seed electrons. However, for PSR and presumably other long-bunch proton machines, the prompt electron signal from electrons striking the wall during a trailing edge multipactor continues to be proportional to the surface density of seed electrons born at the wall from beam losses. This in turn depends very much on the distribution of beam

losses and, in particular, on the grazing angle the protons make with the vacuum chamber surface. It is not practical to measure these to the precision needed.

In principle, beam tracking codes such as ORBIT can model the contribution from scattering of the stored beam in passing through the stripper foil and the generation of halo from space charge effects. In practice, the need for precise knowledge of beam parameters such as closed orbit distortions limits the accuracy of modeling beam losses. Moreover, the contribution to uncontrolled PSR beam losses from the production of excited states of $H^0$ ($n = 3$ and higher) and their subsequent Lorentz stripping in the fringe field of the dipole downstream of the stripper foil is large (15% to 50% of the total losses). The tracking of losses from excited states is very complicated and not included in the present tracking codes.

In light of these difficulties in the simulation of beam losses from first principles, we conclude that seed electrons are probably best inferred from comparison of electron cloud measurements to simulations adjusted for the unknown parameters in the model. Parametric studies in simulations can provide insight into the parameters that have the most effect on the results of interest.

## V. SUMMARY AND CONCLUSIONS

We have developed and successfully tested a new electron cloud diagnostic which can measure both the electron flux striking the vacuum chamber wall and electrons trapped in a quadrupole field. Results obtained using this diagnostic demonstrate that electron cloud generation and trapping in quadrupoles makes a significant contribution to the electron cloud activity in PSR. More specifically, we have found the following important results for PSR: (i) The prompt electron fluxes striking the wall in a quadrupole are comparable to those in an adjacent drift space for the typical beam conditions of the 2006 run cycle at PSR. Since the multipactor gain in the quadrupole is estimated to be down a factor of $\sim 25$, this result implies that primary electron production in the quadrupole is 25 times or so greater than that in the adjacent drift space. (ii) A significant fraction of the electron cloud is trapped in the quadrupole and will survive for a long time after the beam is extracted (exponential life times $\sim 100$ $\mu$s). The observed decay times are in line with simulations using POSINST 12.1. For well-tuned production beams in the 2006 run cycle, we have obtained evidence that a sizable fraction ($> 25\%$) of the electron cloud in the adjacent drift space is seeded by electrons ejected from the adjacent quadrupoles. This result is consistent with the hypothesis that electrons ejected from the quadrupole are the main source of seed electrons in drift spaces. It is also consistent with tracking studies of losses in the ring which show very few grazing angle losses in the drift spaces and in most dipoles but much higher grazing angle losses in the quadrupoles. (iii) The most surprising result, with the electron mirror

in the drift space adjacent to the quadrupole, was the large increase in prompt and swept electron signals in the quadrupole detector when the mirror was biased to more than $-500$ V. The simulation code does not show this effect which suggests that there are some important features missing in the model. (iv) Comparison of a subset of the data with simulations points to the need for more accurate inputs on the distribution of seed electrons from beam losses and a capability to model a section of ring with multiple accelerator components including variation of lattice parameters.

A definitive measurement of the electron cloud seeded only by direct losses in the adjacent drift space is planned for the 2007 run cycle using the two electron longitudinal barriers ("electron mirrors") recently installed on either side of the drift space diagnostic (ES41Y). Electrons ejected from the quadrupoles will be prevented from reaching ES41Y when the electron mirrors are biased to $-2$ kV or more. Additional experiments in 2007 will include rotating the quadrupole diagnostic by 90 degrees to measure the electron cloud generated and trapped in the vertical portion of the quadrupole where beam tracking studies indicate a much higher rate of grazing angle beam losses.

## ACKNOWLEDGMENTS

[1] George P. Lawrence, *Proceedings of the 1987 Particle Accelerator Conference, Washington, DC* (IEEE, Piscataway, NJ, 1987), p. 825.

[2] Robert J. Macek, *Workshop on Space Charge Physics in High Intensity Hadron Rings, Shelter Island, New York*, edited by A. U. Luccio, AIP Conference Proceedings No. 448 (AIP, Woodbury, New York, 1998), p. 116.

[3] D. H. Fitzgerald, R. Garnett, K. Jones, R. J. Macek, F. Merrill, C. Pillai, M. A. Plum, O. R. Sander, A. Browman, D. Johnson, and R. Kustom, *Proceedings of the 1999 Particle Accelerator Conference, New York* (IEEE, Piscataway, NJ, 1999), p. 518.

[4] Lujan Neutron Scattering Center website: http://lansce.lanl.gov/lujan/index.html.

[5] D. Neuffer, E. Colton, D. Fitzgerald, T. Hardek, R. Hutson, R. Macek, M. Plum, H. Thiessen, and T.-S Wang, Nucl. Instrum. Methods Phys. Res., Sect. A **321**, 1 (1992).

[6] R. Macek, A. Browman, D. Fitzgerald, R. McCrady, F. Merrill, M. Plum, T. Spickermann, T. S. Wang, J. Griffin, K. Y. Ng, D. Wildman, K. Harkay, R. Custom, and R. Rosenberg, *Proceedings of the 2001 Particle Accelerator Conference, Chicago, IL* (IEEE, Piscataway, NJ, 2001), p. 688.

[7] R. A. Rosenberg and K. C. Harkay, Nucl. Instrum. Methods Phys. Res., Sect. A **453**, 507 (2000).

[8] R. J. Macek, M. Borden, A. Browman, D. Fitzgerald, T. S. Wang, T. Zaugg, K. Harkay, and R. A. Rosenberg, *Proceedings of the 2003 Particle Accelerator Conference, Portland, OR* (IEEE, Piscataway, NJ, 2003), p. 508.

[9] M. T. F. Pivi and M. A. Furman, Phys. Rev. ST Accel. Beams **6**, 034201 (2003).

[10] M. Plum, J. Allen, M. Borden, D. Fitzgerald, R. Macek, and T. S. Wang, *Proceedings of 1995 Particle Accelerator Conference, Dallas, Texas* (IEEE, Piscataway, NJ, 1996), p. 3406.

[11] M. A. Plum, D. H. Fitzgerald, D. Johnson, J. Langenbrunner, R. J. Macek, F. Merrill, P. Morton, B. Prichard, O. Sander, M. Shulze, H. A. Thiessen, T. S. Wang, and C. A. Wilkinson, *Proceedings of the 1997 Particle Accelerator Conference, Vancouver, Canada* (IEEE, Piscataway, NJ, 1998), p. 1611.

[12] R. J. Macek, Proceedings of ECLOUD'02 Workshop, Geneva, edited by G. Rumolo, p. 259 (CERN-2002-001).

[13] R. J. Macek, A. A. Browman, M. J. Borden, D. H. Fitzgerald, R. C. McCrady, T. Spickermann, and T. J. Zaugg, Proceedings of ECLOUD'04, Napa, California, 2004, edited by M. Furman, p. 63 (CERN-2005-001).

[14] P. Thieberger, A. L. Hanson, D. B. Steski, V. Zajic, S. Y. Zhang, and H. Ludewig, Phys. Rev. A **61**, 042901 (2000).

[15] R. Macek and M. T. F. Pivi, LANL Report, LA-UR-06-0283, 2005.

[16] J. A. Holmes, V. Danilov, J. Galambos, A. Shishlo, S. Cousineau, W. Chou, L. Michelotti, F. Ostiguy, and J. Wei, Proceedings of EPAC02, Paris, France, 2002, p. 1022.

[17] J. D. Galambos, J. A. Holmes, and D. K. Olsen, ORBIT User Manual, Version 1.10, http://neutrons.ornl.gov/APGroup/Codes/orbit.htm.

[18] P. Strubin, "Results from the Scrubbing Run 2004," LHC MAC, 2004, see website http://ab-abp-rlc.web.cern.ch/ab-abp-rlc-ecloud/.

[19] Michel Kireeff Covov, Arthur W. Molvik, Alex Friedman, Jean-Luc Vay, Peter A. Seidl, Grant Logan, David Baca, and Jasmina L. Vujic, Phys. Rev. Lett. **97**, 054801 (2006).

[20] H. Fukuma, J. W. Flanagan, T. Kawamoto, T. Morimoto, K. Oide, M. Tobiiyama, and F. Zimmermann, Proceedings of EPAC 2006, Edinburgh, Scotland, 2006, p. 2901.

[21] R. J. Macek and A. A. Browman, *Proceedings of the 2005 Particle Accelerator Conference, Knoxville, TN, 2005* (IEEE, Piscataway, NJ, 2005), p. 2047.

[22] Y. Sato, *Proceedings of ECLOUD07 Workshop, Daegu, Korea, 2007*, edited by H. Fukuma, E. S. Kim, and K. Ohmi (High Energy Accelerator Research Organization (KEK), Tsukuba-shi, Japan, 2007), p. 196.

[23] Y. Sato, J. Holmes, S. Y. Lee, and R. Macek, *Proceedings of PAC07, Albuquerque, New Mexico, USA* (IEEE, Piscataway, NJ, 2007), p. 3540.